(Received 10 March 2025, Accepted 15 April 2025, Scheduled 26 April 2025)

Research on Lightning-Induced Transient Characteristics of Photovoltaic Power Generation Systems Based on CDEGS

Wen Cao[1], Xiaojun Tang[1], Yicheng Fan[1], Wei Shen[2,*], Bobo Chen[1], and Jiarui Zhang[1]

[1] *School of Electronic Information, Xi'an Polytechnic University, Xi'an 710048, China*
[2] *State Grid Shaanxi Electric Power Company Limited, Xi'an 710199, China*

ABSTRACT: To address the quantification challenges of transient responses in direct lightning strike protection design for photovoltaic (PV) power generation systems, this study establishes an integrated coupled model using CDEGS simulation software, incorporating horizontally layered soil, PV mounting structures, and grounding systems. A comprehensive consideration of key factors, including lightning current waveforms, soil resistivity, and the number of down conductors and vertical grounding electrodes, enables quantitative analysis of transient overvoltage and transient ground potential rise (TGPR) distribution characteristics under varying operating conditions. The results demonstrate that both soil resistivity and lightning current waveforms are critical factors influencing the transient lightning-induced characteristics of PV systems. In typical low-resistivity ($\rho = 200\,\Omega$·m) and high-resistivity ($\rho = 2000\Omega$·m) soil environments, increasing the number of grounding down conductors and vertical grounding electrodes can reduce both induced overvoltage and transient ground potential rise. However, beyond a certain threshold, shielding effects between adjacent grounding bodies limit current dissipation efficiency, leading to diminishing returns. Therefore, PV system lightning protection design must holistically account for soil properties, lightning current parameters, and optimized layout strategies to mitigate transient amplitudes, achieving an optimal balance between lightning protection effectiveness and economic efficiency.

1. INTRODUCTION

Driven by the global energy transition and "dual-carbon" strategy, PV power generation installations have experienced explosive growth. To achieve optimal power generation efficiency, PV systems are often deployed in high-altitude and open areas. However, due to their exposed metal supports and unsheltered environment, lightning has become the primary factor causing damage to PV arrays [1–3]. Statistical analyses indicate that lightning-induced faults account for 26% of system failures, with single strike events potentially incurring economic losses exceeding millions of yuan and triggering regional power outages [4–6]. Lightning poses a threat to system safety through dual pathways: the powerful impulse current generated by a direct lightning strike is injected into the grounding system through the metal supports, causing inductive overvoltage within PV modules that can reach insulation withstand limits, leading to insulation breakdown. Simultaneously, the TGPR formed during lightning current discharge can reach hundreds of kilovolts, causing equipment damage and posing risks of electric shock to personnel through potential gradients [7–9]. As the scale of PV power generation systems continues to expand, equipment damage, system outages, and corresponding economic losses caused by lightning strikes are on the rise. Traditional lightning protection design methods, lacking quantitative analysis of transient coupling processes, struggle to meet the protection requirements in complex electromagnetic environments. Revealing the transient characteristics of lightning strikes has become an urgent need to ensure the safe operation of PV systems [10].

In recent years, scholars have conducted a series of research in various directions within the field of PV lightning protection. Some scholars have utilized measured or simulated experiments to reveal the electrical degradation patterns of PV panels caused by lightning currents. They have observed that under lightning impulse strikes of different stress levels, the peak voltage output of PV panels decreases. However, most of these experiments are based on a single waveform, neglecting the strong randomness and uncertainty of lightning currents [11–13]. Other scholars have established equivalent circuits for PV supports and considered the electromagnetic coupling between various conductors within the array to assess the impact of lightning electromagnetic induction on PV components, but failed to consider the electromagnetic coupling effect between the support structure and grounding system. Furthermore, their studies were all based on uniform soil structures, which deviate from real layered soil conditions [14–17]. There are also scholars who have used simulation methods to reveal the quantitative relationship between soil resistivity and TGPR, and proposed to reduce potential gradients by increasing the number of vertical grounding electrodes. However, they have not addressed the issue of optimizing the compatibility between the number of vertical grounding electrodes and impulse current distribution efficiency [18]. In general, the above studies have analyzed PV supports and grounding systems as independent objects, neglecting the electromagnetic coupling effect between them during lightning-induced transient processes. They lack

* Corresponding author: Wei Shen (47598910@qq.com).

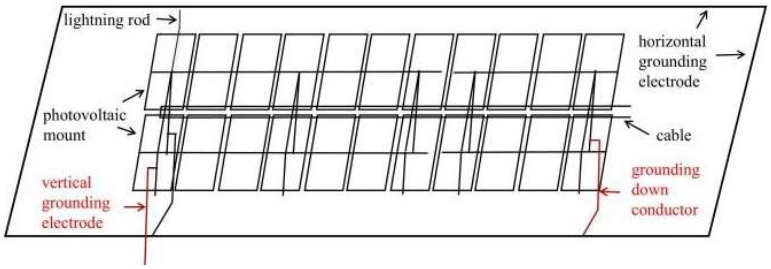

FIGURE 1. Photovoltaic array model.

TABLE 1. Lightning current waveform parameters.

waveform category	first positive lightning strike	first negative lightning strike	subsequent negative lightning strike
waveform parameters	10/350 μs	1/200 μs	0.25/100 μs

comprehensive consideration of the system's overall transient response under different lightning currents and layered soil conditions, resulting in existing protection strategies being unable to accurately predict the system's transient response.

Based on existing research findings and identified gaps, this study employs CDEGS simulation software to establish an integrated model incorporating horizontal double-layer soil, PV support structures, and grounding systems. The research systematically investigates the impacts of critical factors such as lightning current waveforms, soil resistivity, the number of grounding down conductors, and vertical grounding electrodes. Through comparative analysis of transient overvoltage and TGPR distribution patterns under various operating conditions, it provides a quantitative basis for optimizing lightning protection design in PV power systems.

2. SIMULATION MODELING

2.1. Photovoltaic Array Model

As a core component of PV power generation systems, the structural characteristics of PV arrays have a significant impact on the lightning strike transient characteristics of these systems. The lightning transient path of a lightning strike to a PV array is mainly composed of PV supports, which serve as the aboveground supporting structure, and the grounding grid for underground lightning protection, collectively forming a complete path for lightning current discharge [16].

This study employs the HIFREQ module of CDEGS software to establish an integrated PV support-grounding system model, as illustrated in Figure 1. The PV supports consist of multiple branch conductors with complex spatial arrangements, including components such as short posts, long posts, diagonal beams, and crossbeams. Specifically, the short posts are 0.5 m tall; the long posts are 1.7 m tall; and each post base is equipped with a 0.15 m-long concrete pile to enhance the stability and wind resistance of the supports. The diagonal beams measure 1.9 m in length, while the crossbeams are made of 11.4 m-long channel steel, which is equivalent to round steel with a radius of 0.013 m during modeling for easier calculation and analysis. The grounding grid, an essential component of lightning protection for PV arrays, is composed mainly of a combination of vertical grounding electrodes and horizontal grounding electrodes. The grounding grid material is galvanized flat steel with a cross-sectional radius of 0.018 m, buried at a depth of 0.8 m, and covering an area of 20 m × 20 m.

When a lightning strike hits the lightning rod, the lightning current travels along the PV frame and supports, which are typically made of aluminum alloy materials known for their excellent conductivity and corrosion resistance, effectively conducting the lightning current. The lightning current then propagates through the PV frame and supports to the grounding down conductors and ultimately discharged through the grounding grid, ensuring the safe operation of the PV power generation system.

2.2. Lightning Current Model

In lightning protection research, the waveform of the lightning current is a primary parameter indicating the strength of lightning discharge. For the convenience of engineering calculations and quantitative analysis, mathematical formulas are commonly used to fit the lightning current waveform [19]. For simplicity, a double-exponential function formula is employed in simulations to fit the lightning current, with the specific expression being:

$$i(t) = kI_p \left(e^{-\alpha t} - e^{-\beta t}\right) \tag{1}$$

In the formula, k is the peak coefficient; I_p is the peak value of the impulse current waveform; α is the wavefront fitting parameter; and β is the wavetail fitting parameter, all of which are determined by fitting the waveform data.

According to relevant IEC standards [20], Table 1 presents the parameters of several common lightning current waveforms, with the lightning current amplitude uniformly set at 30 kA. The lightning current waveform set using FFTSES in the CDEGS software is shown in Figure 2.

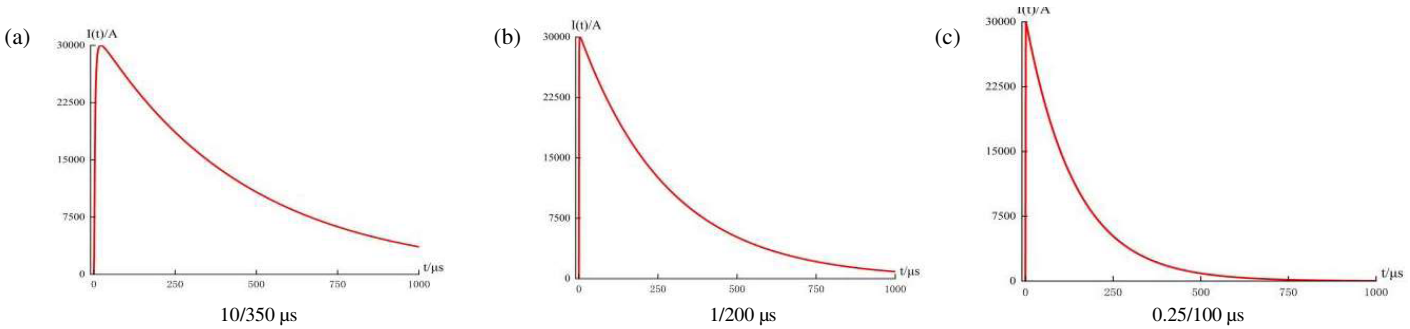

FIGURE 2. Common lightning current waveforms.

2.3. Layered Soil Model

The grounding system serves as the main pathway for lightning current discharge. When designing the grounding system, it is important to note that the grounding electrodes buried underground are not in a single uniform soil environment. The resistivity of the soil varies with depth, which significantly affects the impedance characteristics of the grounding electrodes and, consequently, the performance of the entire grounding system. To accurately assess this impact, this study uses the RESAP module of the CDEGS software to establish a horizontal two-layer soil model and simulates different soil conditions by adjusting the resistivity parameters of the upper soil layer. To ensure the consistency and validity of the model, the thickness of the upper soil layer is set to 5 m, and the lower soil layer is assigned a constant resistivity value of 100 Ω·m. The layered soil model is shown in Figure 3.

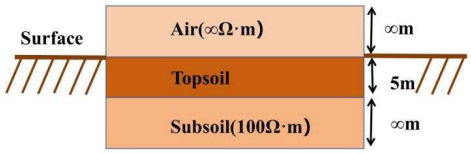

FIGURE 3. Horizontal stratified soil structure model.

3. SIMULATION RESULTS AND ANALYSIS

3.1. Lightning-Induced Transient Characteristics of Photovoltaic Power Generation Systems

This study selects four representative soil types with resistivity values of $\rho = 200\,\Omega$·m (moist clay), $\rho = 500\,\Omega$·m (sandy clay), $\rho = 1000\,\Omega$·m (weathered rock stratum), and $\rho = 2000\,\Omega$·m (dry gravel), along with three standardized lightning current waveforms peaking at 30 kA (0.25/100 μs, 1/200 μs, and 10/350 μs) for comparative analysis.

3.1.1. Induced Overvoltage in Photovoltaic Cables

To analyze the impact of lightning current waveforms and soil resistivity on cable-induced overvoltage, the waveforms of PV cable-induced overvoltage corresponding to three lightning current waveforms under different soil resistivities are plotted, as shown in Figure 4.

As seen in Figure 4, as the lightning transient process continues, the waveform of the cable-induced overvoltage exhibits an oscillating and decaying trend. This is mainly due to the charging and discharging process of the cable's inherent distributed inductance and capacitance to ground, which causes waveform oscillation. The resistance in the cable conductor then damps and attenuates this oscillation, leading to the oscillating and decaying waveform.

Further analysis of the waveforms allowed for the extraction of peak voltage data for the PV cable-induced overvoltage under various lightning current waveforms and soil resistivities. The specific results are shown in Table 2.

TABLE 2. Peak values of induced overvoltage under different soil resistivities and lightning current waveforms.

soil resistivities/Ω·m	peak values of induced overvoltage/kV		
	0.25/100 μs	1/200 μs	10/350 μs
200	54.68	40.06	35.43
500	56.86	40.68	36.82
1000	58.25	43.3	38.79
2000	64.36	48.45	42.24

Figure 5 intuitively demonstrates the trend of the influence of lightning current waveform and soil resistivity on the induced overvoltage in PV cables. It can be observed that, under a fixed soil resistivity condition, when lightning currents with waveforms of 0.25/100 μs, 1/200 μs, and 10/350 μs are injected respectively, the amplitudes of induced overvoltage generated in the PV cables decrease sequentially, indicating a negative correlation between the rise time of the waveform and the amplitude of overvoltage. This is mainly because lightning currents with shorter rise times (such as 0.25/100 μs) contain richer high-frequency components, resulting in more rapid changes in the magnetic field and thus higher induced overvoltage. In addition, soil resistivity mainly affects the dissipation speed and efficiency of lightning currents in the grounding system, with a relatively minor impact on the distribution of electromagnetic fields. As soil resistivity increases, the diffusion of lightning currents is restricted, leading to an increase in local electric field intensity and subsequently a slight increase in induced overvoltage, although this increase is not significant. Data indicate that when soil resistivity increases from 200 Ω·m to 2000 Ω·m,

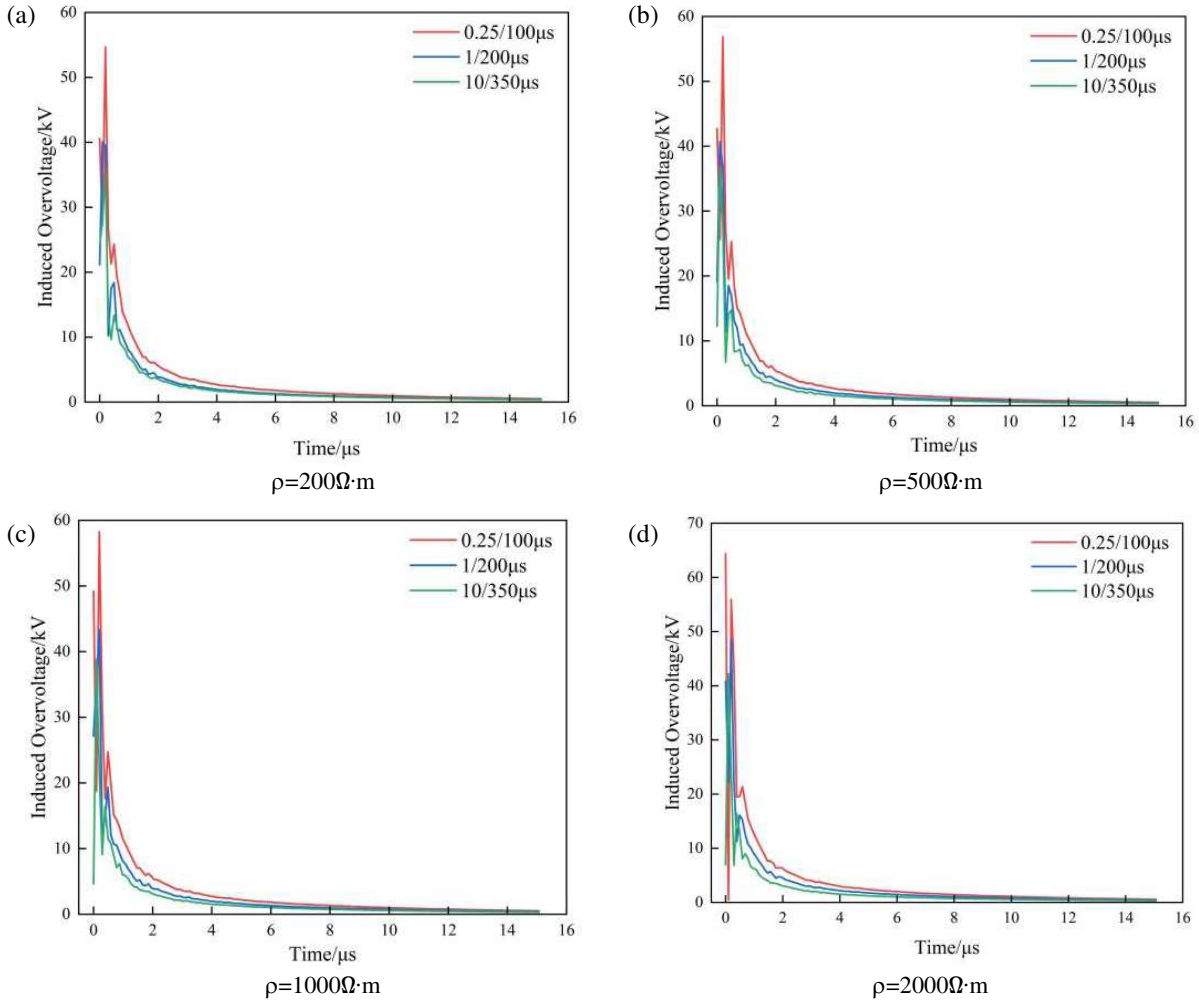

FIGURE 4. Waveforms of induced overvoltage under different soil resistivities and lightning current waveforms.

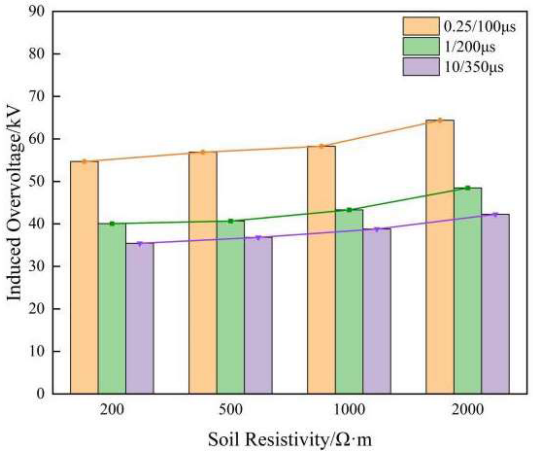

FIGURE 5. Variation trends of induced overvoltage under different soil resistivities and lightning current waveforms.

the induced overvoltage increases by only 17%–20%, whereas shortening the waveform rise time from 10 μs to 0.25 μs results in a surge of over 54% in the peak voltage, proving that the lightning current waveform is the dominant factor.

3.1.2. System TGPR

Taking $\rho = 200\,\Omega$·m (typical medium-to-low resistivity area/wet clay) and $\rho = 2000\,\Omega$·m (high resistivity area/dry gravel) as examples, 3D mapping surface plots of TGPR under different lightning current waveforms were generated to observe the distribution of ground potential rise, as shown in Figures 6 and 7.

As seen in Figures 6 and 7, in low-resistivity soil ($\rho = 200\,\Omega$·m), the distribution of TGPR is relatively uniform, with a gentle 3D surface plot and minimal changes in potential gradient. The peak value is reduced by 50%–62% compared to the scenario in high-resistivity soil ($\rho = 2000\,\Omega$·m), indicating that the lightning current can quickly dissipate into the ground, and the grounding system performs well. However, in high-resistivity soil ($\rho = 2000\,\Omega$·m), due to the limited current dissipation path, the lightning current is forced to concentrate on the grounding conductor or local low-resistivity areas, resulting in abrupt changes in potential gradient and forming a regional high-potential threat.

Through quantitative analysis of TGPR, the peak values of TGPR under different lightning current waveforms and soil resistivity conditions were calculated, with specific data pre-

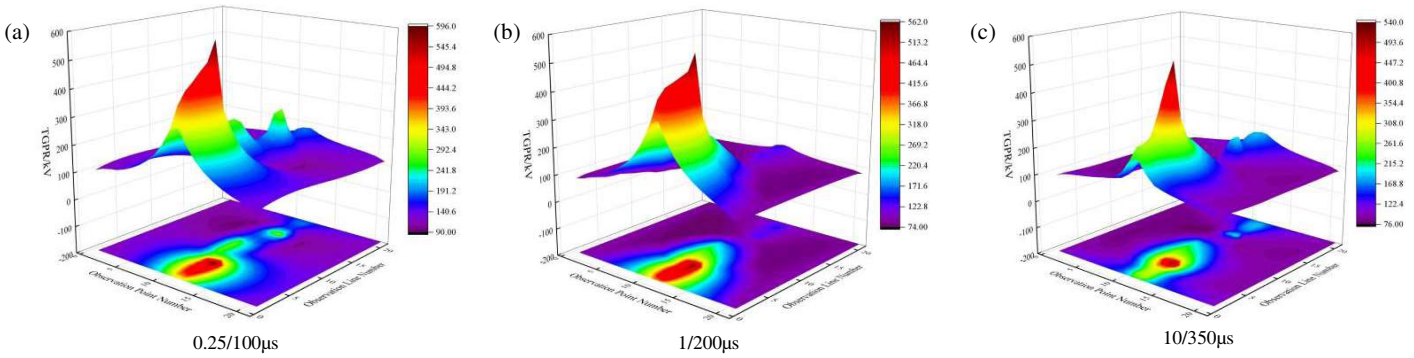

FIGURE 6. Distribution diagram of TGPR at a soil resistivity of 200 Ω·m.

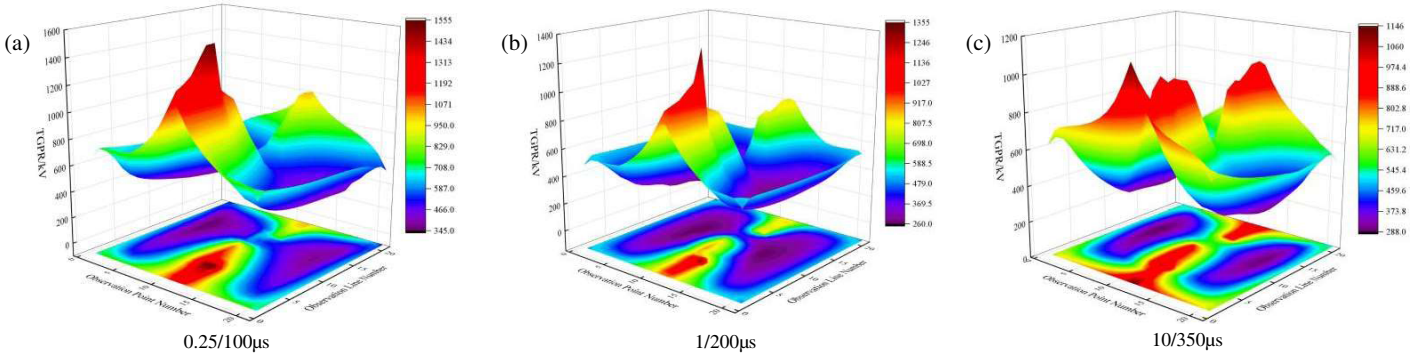

FIGURE 7. Distribution diagram of TGPR at a soil resistivity of 2000 Ω·m.

TABLE 3. Peak values of TGPR under different lightning current waveforms and soil resistivities.

soil resistivities/Ω·m	peak values of TGPR/kV		
	0.25/100 μs	1/200 μs	10/350 μs
200	594.36	560.51	539.6
500	927.67	825.95	688.76
1000	1237.63	1033.41	818.94
2000	1553.91	1353.41	1144.81

sented in Table 3. Additionally, a trend chart of TGPR varying with soil resistivity and lightning current waveforms was plotted, as shown in Figure 8.

As seen in Figure 8, soil resistivity has a significant impact on TGPR: As soil resistivity decreases (e.g., to $\rho = 200\,\Omega$·m), the soil's electrical conductivity improves, allowing the grounding body to disperse lightning currents more effectively, thereby significantly reducing TGPR. Conversely, in areas with high soil resistivity (e.g., $\rho = 2000\,\Omega$·m), the discharge capacity of the grounding system is weaker, resulting in higher TGPR. Additionally, the influence of lightning current waveform cannot be ignored. When the rise time of the lightning current wavefront shortens (e.g., to 0.25/100 μs), TGPR increases significantly. This phenomenon is mainly attributed to the high inductive reactance characteristic of the PV grounding system. As the rise time of the lightning current wavefront shortens, the high-frequency components in the lightning current gradually increase, and the transient impedance of the grounding

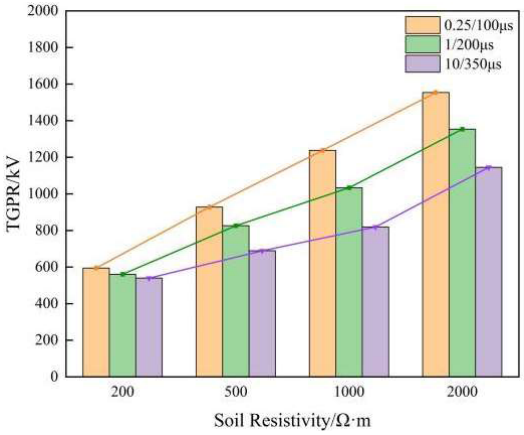

FIGURE 8. Variation trends of TGPR under different lightning current waveforms and soil resistivities.

system at high frequencies correspondingly increases, leading to an increase in the transient potential rise on the grounding body. For instance, under the same soil resistivity condition, the ground potential rise induced by a 0.25/100 μs lightning current waveform is significantly higher than that induced by a 10/350 μs waveform, further validating the significant impact of high-frequency components in lightning currents on TGPR.

Therefore, in practical engineering, the TGPR can be effectively reduced by optimizing soil conductivity, such as using resistance-reducing agents, to enhance the overall lightning protection performance and operational reliability of the system.

TABLE 4. Peak values of induced overvoltage under different numbers of grounding down conductors.

numbers of grounding down conductors	peak values of induced overvoltage/kV					
	$\rho = 200\,\Omega$·m			$\rho = 2000\,\Omega$·m		
	0.25/100 μs	1/200 μs	10/350 μs	0.25/100 μs	1/200 μs	10/350 μs
0	56.81	49.61	32.97	58.92	51.56	34.93
2	37.68	28.6	17.48	40.32	36.04	24.44
4	30.31	27.8	18.93	33.45	31.2	20.5
6	34.94	32.35	18.3	37.02	33.6	20.88
8	31.68	29.53	18.02	36.86	33.46	20.6
10	31.2	29.75	18.73	36.67	33.49	21.01

TABLE 5. Peak values of TGPR under different numbers of grounding down conductors.

numbers of grounding down conductors	peak values of TGPR/kV					
	$\rho = 200\,\Omega$·m			$\rho = 2000\,\Omega$·m		
	0.25/100 μs	1/200 μs	10/350 μs	0.25/100 μs	1/200 μs	10/350 μs
0	638.24	624.64	586.74	3137.92	2501.06	2018.47
2	472.57	449.5	429.45	1897.24	1663.86	1302.73
4	405.85	396.39	372.15	1515.79	1286.54	838.88
6	393.63	369.81	355	1424.99	1180.9	804.01
8	393.1	366.74	345.21	1644.79	1237.71	820.63
10	377.53	365.85	350.95	1528.04	1147.74	806.52

3.2. Impact of the Number of Grounding Down-Conductors

In the lightning protection grounding system of PV power generation systems, the grounding down conductors serve as a crucial bridge connecting the PV support structure to the grounding system. Their topological configuration directly influences the efficiency of lightning current discharge and the transient response characteristics of the system. This study selects $\rho = 200\,\Omega$·m (typical medium-to-low resistivity area/wet clay) and $\rho = 2000\,\Omega$·m (extremely high resistivity area/dry gravel) to establish an extreme geological comparison group, systematically investigating the impact mechanism of the number of down conductors (0/2/4/6/8/10 pieces) on the lightning transient process. The specific data are shown in Tables 4 and 5.

As clearly observed in Figure 9, both the induced overvoltage in PV cables and the TGPR exhibit a gradual decrease with the increase in the number of grounding down conductors. This indicates that increasing the number of grounding down conductors can effectively improve the discharge path of lightning currents and reduce the amplitude of the system's transient response. However, the reduction effect gradually flattens out when the number of down conductors reaches a certain value. For instance, when the number of grounding down conductors increases from 0 to 2, the peak value of induced overvoltage decreases by 30%–47%, and the peak value of TGPR drops by 26%–40%. In contrast, when the number of down conductors increases from 6 to 10, the peak value of induced overvoltage only decreases by about 11%, and the peak value of TGPR only drops by about 7%. This phenomenon is mainly attributed to the shielding effect among the grounding down conductors: when the number of down conductors is small, adding more can significantly improve the grounding body's ability to discharge lightning currents. However, as the number of down conductors increases to a certain extent, the distance between them decreases, enhancing the electromagnetic shielding effect among them, which results in further increase in the number of down conductors having a less significant effect on reducing induced overvoltage and TGPR.

3.3. Impact of the Number of Vertical Grounding Electrodes

By increasing the soil contact area and improving the impulse ionization effect, vertical grounding electrodes can significantly enhance the efficiency of lightning current discharge. Their configuration strategies directly affect the impulse current distribution efficiency and transient electromagnetic energy distribution characteristics. This study selects $\rho = 200\,\Omega$·m (typical medium-to-low resistivity area/wet clay) and $\rho = 2000\,\Omega$·m (extremely high resistivity area/dry gravel) to establish an extreme geological comparison group, systematically investigating the regulation mechanism of the number of vertical grounding electrodes (0/2/4/6/8/10 pieces) on the lightning transient process. The specific data are shown in Tables 6 and 7.

Figure 10 intuitively demonstrates the impact of the number of vertical grounding electrodes on the variation trends of cable-induced overvoltage and TGPR. It can be clearly observed that, as the number of vertical grounding electrodes increases, the amplitudes of both the induced overvoltage and TGPR decrease significantly compared to the case with no vertical grounding electrodes. This indicates that increasing the number of ver-

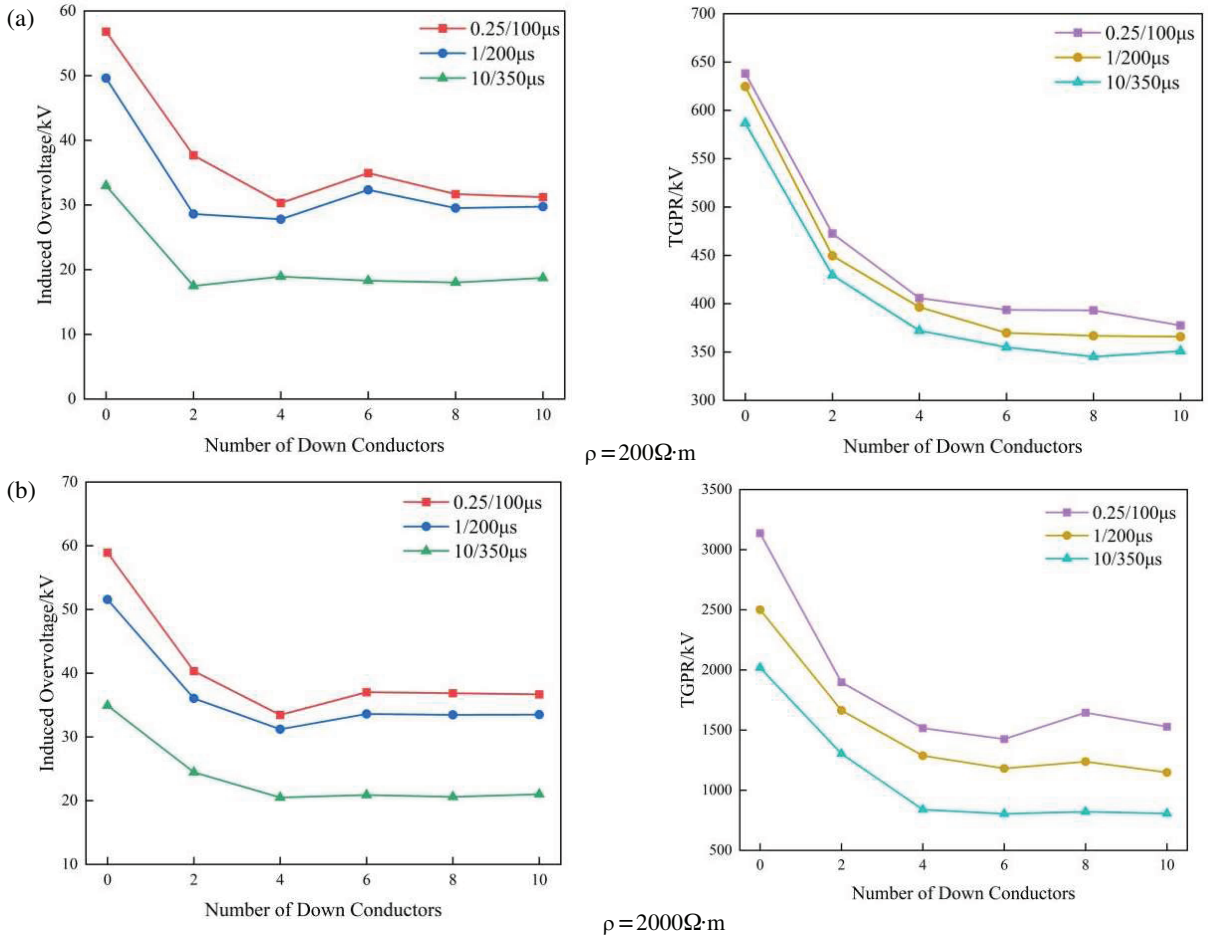

FIGURE 9. Variation patterns of transient characteristics under different numbers of grounding down conductors.

TABLE 6. Peak values of induced overvoltage under different numbers of vertical grounding electrodes.

numbers of vertical grounding electrodes	peak values of induced overvoltage/kV					
	$\rho = 200\,\Omega$·m			$\rho = 2000\,\Omega$·m		
	0.25/100 μs	1/200 μs	10/350 μs	0.25/100 μs	1/200 μs	10/350 μs
0	54.68	40.06	35.43	64.36	48.45	42.24
2	33.63	26.85	19.56	41.32	30.46	26.22
4	21.72	15.85	11.58	35.36	21.89	14.11
6	19.23	13.89	7.71	25.64	24.34	15.9
8	19.19	13.26	9.64	25.62	23.95	15.26
10	18.89	13.12	9.46	25.11	23.55	15.05

tical grounding electrodes can effectively improve the current dissipation capacity of the grounding system and reduce the amplitude of the system's transient response. Additionally, the reduction effect tends to flatten out when the number of vertical grounding electrodes reaches a certain value. For instance, when the number of vertical grounding electrodes increases from 0 to 4, the amplitude of induced overvoltage decreases by 45%–67%, and the amplitude of TGPR drops by 22%–33%. However, when the number of vertical grounding electrodes increases from 6 to 10, the amplitude of induced overvoltage only decreases by 2%–6%, and the amplitude of TGPR decreases by approximately 3%. This suggests that there is a saturation point in the effect of increasing the number of vertical grounding electrodes on reducing induced overvoltage and TGPR. This phenomenon is mainly attributed to the shielding effect among the vertical grounding electrodes: when the number of vertical grounding electrodes is small, adding more electrodes can significantly expand the contact area between the grounding system and the soil, improving the discharge path for lightning currents. However, when the number of vertical grounding electrodes increases to a certain extent, the distance between them decreases, enhancing the electromagnetic shielding effect

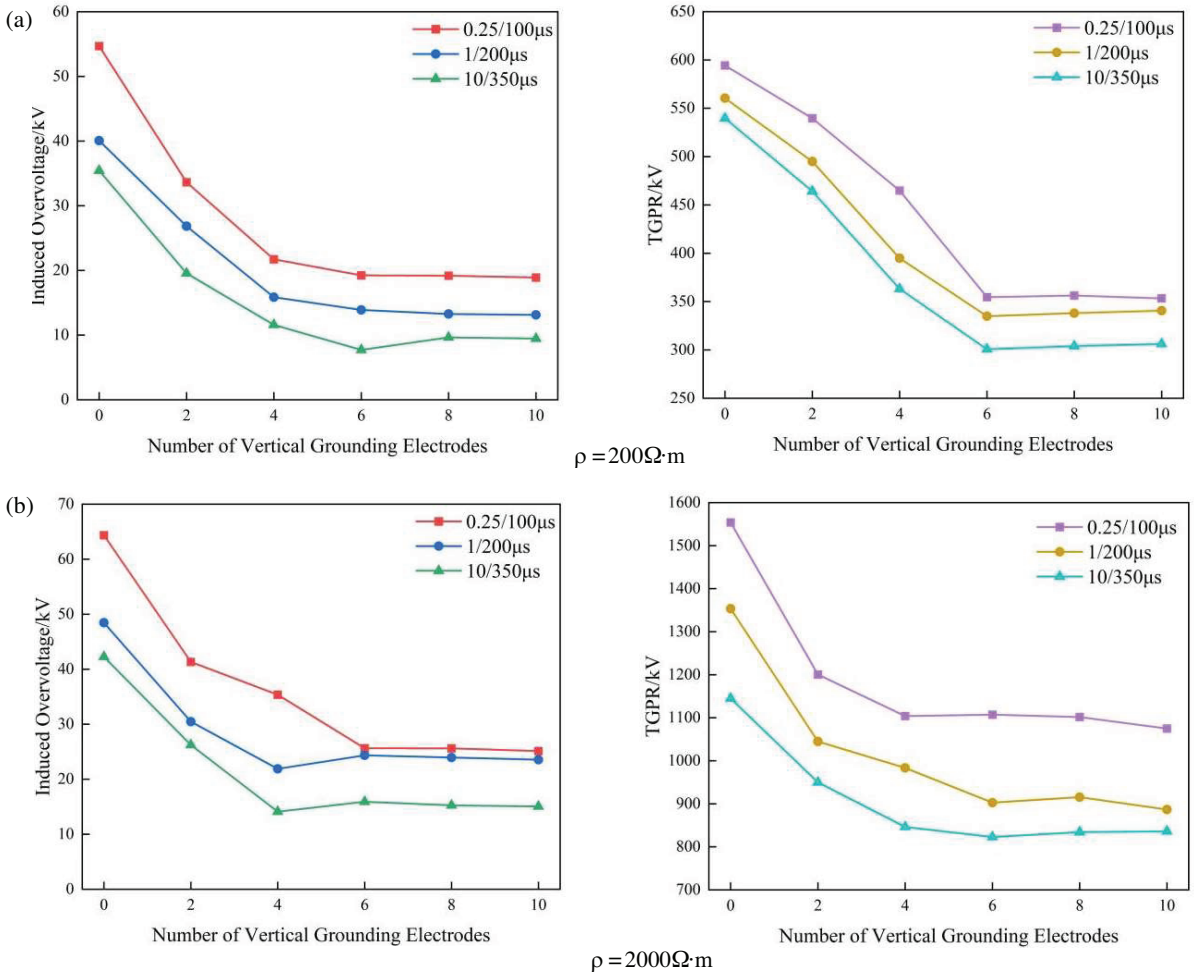

FIGURE 10. Variation patterns of transient characteristics under different numbers of vertical grounding electrodes.

TABLE 7. Peak values of TGPR under different numbers of vertical grounding electrodes.

numbers of vertical grounding electrodes	peak values of TGPR/kV					
	$\rho = 200\,\Omega$·m			$\rho = 2000\,\Omega$·m		
	0.25/100 μs	1/200 μs	10/350 μs	0.25/100 μs	1/200 μs	10/350 μs
0	594.36	560.51	539.6	1553.91	1353.41	1144.81
2	539.6	494.95	464.15	1200.41	1044.81	949.78
4	464.79	394.89	363.19	1103.99	983.41	846.11
6	354.56	334.9	300.75	1107.22	902.66	822.78
8	356.23	338.05	303.96	1101.7	915.51	834.13
10	353.3	340.66	306.31	1074.92	886.55	835.87

among them. This results in a smaller current dissipation range when multiple electrodes dissipate current simultaneously compared to when they act individually, thereby limiting the effect of further reducing induced overvoltage and TGPR.

4. CONCLUSION

This study establishes an integrated joint model encompassing horizontal two-layer soil, PV supports, and grounding systems using the CDEGS simulation software. It comprehensively considers the key factors such as lightning current waveform, soil resistivity, grounding down conductors, and the number of vertical grounding electrodes, and quantitatively analyzes the distribution patterns of induced overvoltage and TGPR under different operating conditions. The following conclusions are drawn through simulation analysis:

a) Due to the cable's inherent resistance, distributed inductance, and capacitance to ground, the induced overvoltage waveform generated in the cable under lightning impulses exhibits an oscillatory decay trend. Compared to

soil resistivity, the wavefront time of the lightning current plays a dominant role in determining the amplitude of the induced overvoltage. Specifically, the shorter the wavefront time is, the higher the proportion of high-frequency components is in the lightning current, and the faster the transient change rate of the spatial magnetic field is. This results in a significant increase in the amplitude of the induced overvoltage coupled onto the PV cable. Conversely, an increase in soil resistivity increases the impedance of the grounding system, indirectly enhancing the magnetic field intensity around the lightning current discharge path, causing the induced overvoltage to show a slight upward trend. However, the degree of this impact is much weaker than the wavefront time parameter.

b) Soil resistivity and lightning current waveform are two key factors influencing TGPR. Specifically, in low-resistivity soil (200 Ω·m), the TGPR distribution is relatively uniform with a gentle potential gradient change, and its peak value decreases by 50%–62% compared to scenarios in high-resistivity soil (2000 Ω·m). This indicates that in low-resistivity soil environments, the lightning current discharge efficiency is higher, and the transient performance of the grounding system is good. Conversely, in high-resistivity soil ($\rho = 2000\,\Omega\cdot$m), the current dispersion path is limited, forcing the lightning current to concentrate on the grounding conductor or locally low-resistivity areas, resulting in sharp changes in potential gradient and the formation of localized high-potential threats. Furthermore, as the current wavefront time decreases, the skin effect is induced due to the increased proportion of high-frequency current components, leading to an increase in the transient impedance of the grounding system and thereby significantly elevating the TGPR amplitude. Therefore, in practical engineering, optimizing soil conductivity, such as by using resistance-reducing agents, can effectively reduce TGPR.

c) In both typical scenarios of low soil resistivity areas ($\rho = 200\,\Omega\cdot$m) and high soil resistivity areas ($\rho = 2000\,\Omega\cdot$m), increasing the number of grounding down conductors and vertical grounding electrodes can effectively reduce the amplitudes of both induced overvoltage and TGPR. However, it should be noted that due to the shielding effect between grounding electrodes, the current distribution range when multiple grounding electrodes are acting simultaneously is smaller than when they are acting individually, leading to a gradual leveling off of the improvement in current distribution effectiveness. For example, when the number of grounding down conductors increases from zero to two, the peak value of induced overvoltage decreases by 30%–47%, and the peak value of TGPR decreases by 26%–40%. However, when the number of down conductors increases from six to ten, the peak value of induced overvoltage only decreases by about 11%, and the peak value of TGPR only decreases by about 7%. Similarly, when the number of vertical grounding electrodes increases from zero to four, the amplitude of induced overvoltage decreases by 45%–67%, and the amplitude of TGPR decreases by 22%–33%. Nevertheless, when the number of vertical grounding electrodes increases from six to ten, the amplitude of induced overvoltage only decreases by 2%–6%, and the amplitude of TGPR only decreases by about 3%.

Therefore, in practical engineering, it is advisable to avoid blindly increasing the number of grounding down conductors and vertical grounding electrodes. Instead, scientific design and optimized layout should be adopted to reduce the amplitude of the lightning-induced transient characteristics of PV power generation systems. This not only enhances the lightning protection performance of the PV power generation system but also reduces engineering costs and maintenance difficulties while ensuring safety and reliability.

ACKNOWLEDGEMENT

This research was financially supported by Key Research and Development Program of Shaanxi (No. 2024GX-YBXM-519) and National Engineering Research Center of UHV Technology and Novel Electrical Equipment Basis (No. NERCUHE-2024-KF-14).

REFERENCES

[1] Fang, R. C., J. Yang, K. Zhou, *et al.*, "An optimal planning method for park ies considering life cycle carbon cost," *Electric Power*, Vol. 55, No. 12, 135–146, 2022.

[2] Zhao, X.-G., W. Wang, and L. Wu, "A dynamic analysis of research and development incentive on china's photovoltaic industry based on system dynamics model," *Energy*, Vol. 233, 121141, 2021.

[3] Ogbonnaya, C., A. Turan, and C. Abeykoon, "Novel thermodynamic efficiency indices for choosing an optimal location for large-scale photovoltaic power generation," *Journal of Cleaner Production*, Vol. 249, 119405, 2020.

[4] Apolinskiy, M. I., V. Y. Frolov, A. D. Sivaev, and E. Y. Enkin, "Analysis of the arc quenching system of an arrester operation based on a flow ultrasound generator," *Energies*, Vol. 17, No. 19, 4975, 2024.

[5] Formisano, A., C. Petrarca, J. C. Hernández, and F. J. Muñoz-Rodríguez, "Assessment of induced voltages in common and differential-mode for a PV module due to nearby lightning strikes," *IET Renewable Power Generation*, Vol. 13, No. 8, 1369–1378, June 2019.

[6] Liu, L. G. and C. L. Ma, "A dc bias current reducing method considering grounding electrode location and receiving-end grid structure," *Electric Power*, Vol. 54, No. 7, 100–108, 2021.

[7] Dong, X., Z. Hua, L. Shang, B. Wang, L. Chen, Q. Zhang, *et al.*, "Morphological characteristics and technology prospect of new distribution system," *High Voltage Engineering*, Vol. 47, No. 09, 3021–3035, 2021.

[8] Ogbonnaya, C., A. Turan, and C. Abeykoon, "Novel thermodynamic efficiency indices for choosing an optimal location for large-scale photovoltaic power generation," *Journal of Cleaner Production*, Vol. 249, 119405, 2020.

[9] Pei, Z. Y., Z. F. Liang, W. H. Lu, *et al.*, "Wide-area distributed photovoltaic power generation monitoring and output estimation," *Electric Power*, Vol. 53, No. 6, 87–96, 2020.

[10] Xia, Z., Y. Li, R. Chen, D. Sengupta, X. Guo, B. Xiong, and Y. Niu, "Mapping the rapid development of photovoltaic power

stations in northwestern china using remote sensing," *Energy Reports*, Vol. 8, 4117–4127, 2022.

[11] Zhong, X., Q. Sun, J. Zhang, L. Yang, J. Yang, T. Yang, and L. Fang, "A novel transient model of photovoltaic module considering electromagnetic coupling," *IEEE Journal of Photovoltaics*, Vol. 13, No. 1, 122–132, 2022.

[12] Sabiha, N. A., M. Alsharef, M. K. Metwaly, E. E. Elattar, I. B. M. Taha, and A. M. Abd-Elhady, "Sustaining electrification service from photovoltaic power plants during backflow lightning overvoltages," *Electric Power Systems Research*, Vol. 186, 106386, 2020.

[13] Zhang, Y., H. Chen, and Y. Du, "Considerations of photovoltaic system structure design for effective lightning protection," *IEEE Transactions on Electromagnetic Compatibility*, Vol. 62, No. 4, 1333–1341, 2020.

[14] Zhang, Y., B. Li, Y. Du, Y. Ding, J. Cao, and J. Lv, "Effective grounding of the photovoltaic power plant protected by lightning rods," *IEEE Transactions on Electromagnetic Compatibility*, Vol. 63, No. 4, 1128–1136, 2021.

[15] Young, J. C., K. K. Ho, and J. L. Yun, "Influence of lightning surge on photovoltaics considering lpz protection level and iec-60364 grounding system," *The Transactions of the Korean Institute of Electrical Engineers*, Vol. 68, No. 11, 1288–1291, 2019.

[16] Wang, Y., X. Zhang, and S. Tao, "Modeling of lightning transients in photovoltaic bracket systems," *IEEE Access*, Vol. 7, 12 262–12 271, 2019.

[17] Wang, Y., X. Zhang, and S. Tao, "Numerical method for lightning transient analysis of photovoltaic bracket systems," *Journal of Renewable and Sustainable Energy*, Vol. 12, No. 3, 033501, 2020.

[18] Naxakis, I., E. Pyrgioti, V. Perraki, and E. Tselepis, "Studying the effect of the impulse voltage application on sc-si pv modules," *Solar Energy*, Vol. 144, 721–728, 2017.

[19] Hu, D. F., H. S. You, and X. L. Hao, "Lightning protection for tianjin national convention & exhibition center," *Building Science*, Vol. 36, No. 9, 86–91, 2020.

[20] IEC 62305-1, "Protection against lightning — Part 1: General principles," *International Standard*, International Electrotechnical Commission, 2010.